Wide-range line shape control of Fano-like resonances in all-dielectric multilayer structures based on enhanced light absorption in photochromic waveguide layers

Motokura, Kengo ; Kang, Byungjun ; Fujii, Minoru ; Nesterenko, Dmitry, V ; Sekkat, Zouheir ; Hayashi, Shinji

(Citation)
Journal of Applied Physics,127(7):073103-073103

(Issue Date)
2020-02-21

(Resource Type)
journal article

(Version)
Version of Record

Journal of Applied Physics

Wide-range line shape control of Fano-like resonances in all-dielectric multilayer structures based on enhanced light absorption in photochromic waveguide layers

Cite as: J. Appl. Phys. **127**, 073103 (2020); https://doi.org/10.1063/1.5131681
Submitted: 15 October 2019 . Accepted: 28 January 2020 . Published Online: 18 February 2020

Kengo Motokura, Byungjun Kang, Minoru Fujii, Dmitry V. Nesterenko, Zouheir Sekkat, and Shinji Hayashi

Journal of Applied Physics ARTICLE scitation.org/journal/jap

Wide-range line shape control of Fano-like resonances in all-dielectric multilayer structures based on enhanced light absorption in photochromic waveguide layers

Cite as: J. Appl. Phys. **127**, 073103 (2020); doi: 10.1063/1.5131681
Submitted: 15 October 2019 · Accepted: 28 January 2020 ·
Published Online: 18 February 2020

Kengo Motokura,[1] Byungjun Kang,[1] Minoru Fujii,[1] Dmitry V. Nesterenko,[2,3] Zouheir Sekkat,[4,5,6] and Shinji Hayashi[1,4,a)]

AFFILIATIONS

[1]Department of Electrical and Electronic Engineering, Graduate School of Engineering, Kobe University, Kobe 657-8501, Japan
[2]Image Processing Systems Institute RAS—Branch of the FSRC "Crystallography and Photonics" RAS, Samara 443001, Russia
[3]Faculty of Information Technology, Samara National Research University, Samara 443086, Russia
[4]Optics and Photonics Center, Moroccan Foundation for Science, Innovation and Research (MAScIR), Rabat 10100, Morocco
[5]Faculty of Sciences, Mohammed V University in Rabat, Rabat 10010, Morocco
[6]Graduate School of Engineering, Osaka University, Suita 565-0871, Japan

[a)]**Author to whom correspondence should be addressed:** s.hayashi@dragon.kobe-u.ac.jp

ABSTRACT

We have succeeded in controlling the line shape of Fano-like resonances in all-dielectric multilayer structures in a wide range by UV light irradiation. Multilayer structures consisting of a waveguide layer supporting a half-leaky guided mode, a spacer layer, and another waveguide layer supporting a planar waveguide mode are known to exhibit Fano-like line shapes in attenuated total reflection spectra due to coupling between the half-leaky guided mode and the planar waveguide mode. Using a photochromic layer, i.e., a layer doped with spiropyran molecules, as one of the waveguide layers, we controlled the amount of light absorption in the waveguide layer by varying the UV irradiation dose. We demonstrated that the line shape changes dramatically depending on the UV dose, from the electromagnetically induced transparency-like to electromagnetically induced absorption-like line shape (or vice versa) passing through the Fano-like line shape. We also demonstrated that the photochromic response induced by UV irradiation in the Fano-resonant multilayer structure is enhanced by a factor of ~100 relative to that in a single photochromic layer. Our analyses based on electromagnetic calculations suggest that the dramatic line shape change and the enhanced photochromic response are the consequences of enhanced local electric fields inside the photochromic waveguide layer combined with the photoinduced increase in the imaginary part of the dielectric constant.

I. INTRODUCTION

In atomic systems, peculiar spectral line shapes associated with Fano resonance,[1,2] electromagnetically induced transparency (EIT),[3–5] and electromagnetically induced absorption (EIA)[6–8] have been the subject of extensive experimental and theoretical studies. Asymmetric line shapes observed in atomic spectra were analyzed by Fano and explained in terms of the interference between a discrete level and a continuum.[1,2] He derived a line shape function, called Fano function, which describes the asymmetric line shape with the aid of an asymmetric parameter. The EIT and EIA are inherently quantum mechanical effects leading to a narrow transmission window in a broad absorption band and a narrow absorption peak superposed on a broad absorption band, respectively. They are the consequences of a quantum interference of two excitation pathways of coherent atomic states induced by pump light.[3–8] Over the past decade, great effort has been made to realize the classical analogs of the above quantum effects in photonic nanostructures. For a variety of photonic nanostructures, including

metamaterials and photonic crystals composed of plasmonic (metallic) as well as dielectric building blocks, Fano-like,[9–11] EIT-like,[12–15] and EIA-like[16,17] line shapes in optical spectra have been reported. In these photonic nanostructures, the peculiar line shapes have commonly been explained in terms of the interference between a broad electromagnetic (EM) mode, usually a bright mode with a large radiation loss such as an electric dipole mode, and a sharp EM mode, usually a dark mode with a small radiation loss such as an electric quadrupole mode and a magnetic dipole mode. The Fano-like, EIT-like, and EIA-like resonances with high quality (Q) factors in tailored photonic nanostructures are very much promising for developing potential applications including chemical or biological sensing,[18,19] optical switching,[20,21] and platforms of enhanced spectroscopy.[22–28]

It is well known that a metal–dielectric interface can support surface plasmon polariton (SPP) modes[29] and a high-index dielectric layer cladded by low-index dielectrics can support planar waveguide (PWG) modes.[30] Since these EM modes are nonradiative modes characterized by dispersion relations lying outside the light cone in the ω (angular frequency) $- k_{\|}$ (in-plane wavevector) space, they cannot be excited directly by light propagating in the surrounding medium. The attenuated total reflection (ATR) method is one of the most frequently used methods for exciting these modes, in which a multilayer sample is attached to a high-index prism, and the modes are excited by evanescent waves generated by the prism under the total internal reflection condition.[29] In recent years, there has been a growing interest in the classical analogs of Fano resonance, EIT, and EIA appearing in planar multilayer systems. In fact, Grotewohl and Deutsch[31] predicted the emergence of the Fano-like line shapes in the angle-scan ATR spectra of metal–insulator–metal (MIM) stacks based on EM calculations. Such Fano-like line shapes as well as EIT-like and EIA-like line shapes have been experimentally observed in the angle-scan ATR spectra of an MIM structure consisting of Au, SiO_2, and Ag layers by Tomita *et al.*[32–34] These line shapes are known to originate from the coupling between a metal-clad dielectric waveguide mode (broad mode) and an SPP mode (sharp mode).

Over the past five years, we have carried out theoretical and experimental studies on the Fano-like resonances in metal-dielectric[35–39] and all-dielectric multilayer structures.[40] From analytical EM calculations, we showed that in metal-multilayer structures, the Fano-like line shape originates from the coupling between a broad SPP mode and a sharp PWG mode, while in all-dielectric multilayer structures, the coupling between a broad PWG mode and a sharp PWG mode leads to the Fano-like line shape. We experimentally demonstrated that the line shape can easily be controlled by changing the structural parameters, enabling us to realize sharp resonances with Q values as high as ~3000.[40] Our numerical calculations suggested that the sensitivity of conventional surface plasmon resonance sensors based on the SPP excitation can be increased by several orders of magnitude when the conventional sensor head is replaced by the Fano-resonant metal–dielectric multilayer structures.[36,37] We have also succeeded in light control of the Fano-like resonance using waveguide layers doped with photochromic molecules, namely, disperse red 1 (DR1) molecules. In a metal–dielectric multilayer structure that contains a DR1-doped dielectric waveguide layer, we demonstrated active tuning of the position of the Fano-like resonance upon blue light irradiation.[41–43] Furthermore, in an all-dielectric multilayer structure that also contains a DR1-doped dielectric waveguide layer, we demonstrated systematic changes in the line shape caused by blue light irradiation.[44]

In exactly the same context as the active control of plasmonic resonances (active plasmonics[45]) and electric and magnetic resonances in dielectric nanostructures,[46] the active control of the Fano-like, EIT-like, and EIA-like resonances is extremely important to push forward the resonances to real applications, such as optical modulators, switches, and circuits. During the past few years, attempts to control the Fano-like and EIT-like resonances by mechanical stresses,[47] electric fields,[48–50] temperature,[51–53] and light[41,42,44,54–56] have been reported. However, in spite of the great efforts devoted so far, the active control of the resonances in photonic structures is still at the initial stage, and further experimental and theoretical studies are highly required. Although we have demonstrated the tuning and line shape control of the Fano-like line shape by light irradiation in the multilayer structures containing the photochromic layer,[41,42,44] the dynamical range of light control achieved was very small.

Motivated by previous reports on the successful active control of strong light–matter coupling[57] and plasmonic resonances[58,59] based on photochromic responses of spiropyran (SP) molecules, we extended our previous work[41,42,44] to realize a wide-range control of the Fano-like resonance in all-dielectric structures. In this paper, we show that incorporation of a waveguide layer doped with SP molecules into the multilayer structures makes it possible to change continuously the ATR line shape by UV irradiation from the EIT-like to EIA-like line shape passing through the Fano-like line shape, which was not possible in the previous work. Our results of EM calculations suggest that the wide controllability of the line shape stems from a large change in the extinction coefficient of the SP-doped waveguide layer combined with highly enhanced local electric fields inside the waveguide layer. We also demonstrate that the SP-doped photochromic layer incorporated in the multilayer structure leads to photochromic responses much larger than those achieved by the single layer.

II. EXPERIMENTAL

The Fano-resonant multilayer structure used in the present work is schematically shown in Fig. 1(a). A stack of three dielectric layers was prepared on a glass substrate and attached to a high-index prism to construct a Kretschmann ATR configuration. The surrounding medium is air. The structure of the sample is very similar to that used in our previous work of light-controllable Fano-like resonance.[44] Since both the prism and the substrate are made of SF11 glass and the multilayer structure is attached to the prism with the aid of index matching fluid, the substrate can be regarded as a part of the prism. We denote the complex refractive indices of the prism, ith layer ($i = 1, 2, 3$), and air, as N_p, N_i, and N_a, respectively. To denote the refractive indices n and the extinction coefficients κ of respective media, we use the same subscripts, like $N_i = n_i + i\kappa_i$ for the ith layer. In the present work, materials of the layers were selected such that the refractive indices satisfy the relationships $n_p > n_1 > n_2$, $n_p > n_3$ and $n_3 > n_2 > n_a$. Note that the same relationships were satisfied in the samples used in our previous work.[44]

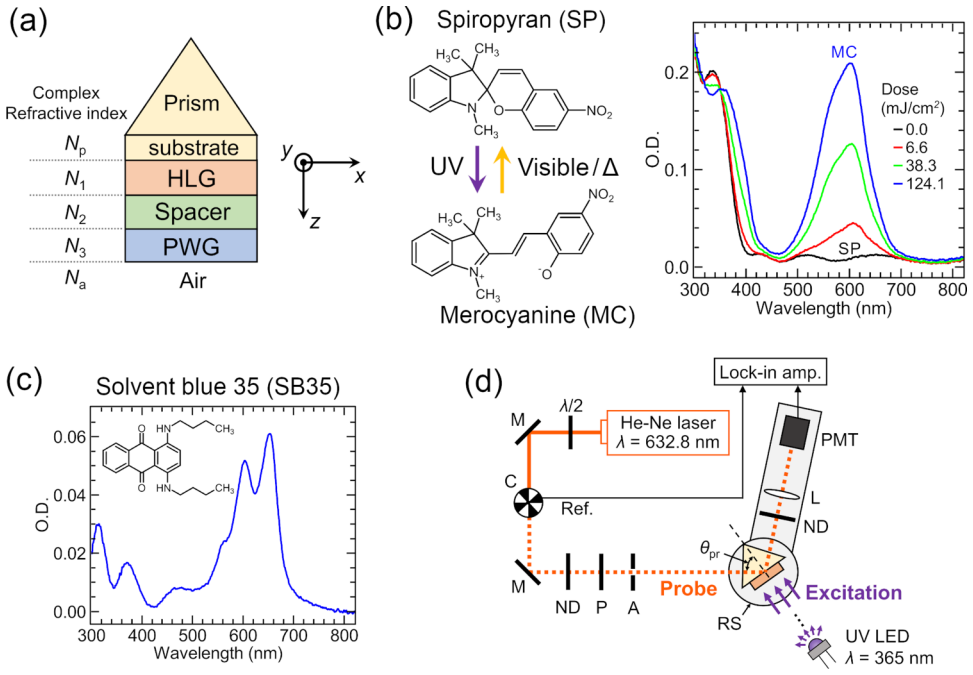

FIG. 1. (a) Sample composed of a HLG layer, a Spacer layer, and a PWG layer, attached to a prism in Kretschmann ATR configuration. (b) Molecular structures of spiropyran (SP) and merocyanine (MC) and the optical density (O.D.) spectra of the SP-PS monolayer measured after UV irradiation with various doses. (c) Molecular structure of solvent blue 35 (SB35) and the O.D. spectrum of SB35-PS single layer. (d) Optical setup used for ATR measurements. Optical elements used are half wave plate ($\lambda/2$), mirror (M), chopper (C), neutral density filter (ND), polarizer (P), aperture (A), rotation stage (RS), lens (L), and photomultiplier (PMT). The sample surface was irradiated uniformly by UV light from a UV-LED placed at a long distance.

Under the condition of $n_3 > n_2$, n_a, it is well known that the third layer with n_3 can support PWG modes;[30] a PWG mode is an EM wave that propagates inside the waveguide layer in a planar direction [x direction in Fig. 1(a)] and accompanies evanescent fields inside the adjacent layers. When $n_p > n_1 > n_2$ holds, the first layer with n_1 can support the so-called half-leaky guided (HLG) modes, which propagate inside the layer along the planar direction and accompany the evanescent fields inside the second layer with n_2 and a traveling wave inside the prism.[60,61] When both the HLG and PWG modes are excited simultaneously in the present multilayer structure, they can interact with each other through the evanescent fields inside the second layer (spacer layer). In the previous work,[44] we have shown that the interaction between the HLG and PWG modes is responsible for generating the Fano-like line shapes in the ATR spectra. It should be noted that the Fano-like line shapes reported in the present paper are generated by the same mechanism. Hereafter, we call the three layers as HLG, Spacer, and PWG layers, respectively, as indicated in Fig. 1(a).

To control the ATR line shape by light irradiation, a polystyrene (PS) layer doped with SP molecules, denoted as the SP-PS layer, was implemented as for the HLG or PWG layer. As described in detail in the literature,[62–65] SP molecules are photochromic molecules that undergo the photochemical reaction shown in the left panel of Fig. 1(b). A closed-ring form of the molecule, which is a stable form, exhibits an absorption band in the UV region (between 320 and 400 nm) and is thus colorless. Upon UV light irradiation, the cleavage of the C–O bond takes place, leading to the transformation of the molecule into the open-ring colored form, i.e., merocyanine (MC), which shows a strong absorption band in the visible region (500–600 nm). Irradiation of the MC molecule by visible light induces backconversion to the close-ring colorless form. Note that the backconversion from MC to SP also takes place thermally in the dark because the open-ring MC form is thermodynamically unstable.

A variety of potential applications have been developed so far by incorporating the SP molecules into polymeric host materials.[57–59,66,67] In the present work, we used PS as the host material.[68] In the right panel of Fig. 1(b), the typical absorption spectra of a single SP-PS layer (SP/PS = 10 wt. %) deposited on a glass substrate observed before and after irradiation of UV light with various doses are presented. We measured the spectra by a UV-visible spectrophotometer (Shimadzu UV-3101PC); a UV light-emitting diode (LED) (NICHIA, NVSU233A) with a wavelength of 365 nm was used as a UV light source. As can be seen from the figure, before UV irradiation, the single SP-PS layer exhibits no absorption band in the visible region. However, after UV irradiation, the layer exhibits a broad absorption band peaking around 600 nm and the absorption band grows as the UV dose increases. The spectra presented in Fig. 1(b) are very similar to those reported by Sasaki and Nagamura.[68] A very weak shoulder is seen at the short-wavelength side of the absorption maximum. According to our detailed studies performed by varying the SP concentration and UV dose, the weak shoulder is thought to be a signature of the initial stage of MC stack formation toward the formation of H-aggregates.[65,69] Figure 1(b) demonstrates that the absorption in the SP-PS layer in the visible range can easily be controlled by UV irradiation. We apply this photochromic effect to control the ATR line shape by incorporating the SP-PS layer in our multilayer samples as the HLG or PWG layer.

Since the ATR response of the multilayer structure is determined by the total amount of light absorption in the structure,[40,44] controlling the absorption in each layer is crucial to achieve a full

control of the ATR line shape. In addition to the photochromic layer, we implemented an absorptive layer used either as the HLG layer or PWG layer. The absorptive layer was prepared by doping solvent blue 35 (SB35) dye molecules into a PS layer. A typical absorption spectrum of a SB35-doped PS (SB35-PS) layer measured by a UV-visible spectrophotometer (Shimadzu UV-3101PC) is shown in Fig. 1(c). We see that the SB35-PS layer exhibits a large absorption band in the green–red region. It should be noted that SB35 molecules are not photoreactive; we confirmed that the absorption spectrum of the SB35-PS layer is unchanged even when the layer is exposed to strong UV light for more than 5 min. As for the Spacer layer, a polyvinyl alcohol (PVA) layer, which is transparent and not photoreactive, was used. Our strategy is to modulate the HLG mode or the PWG mode individually by light irradiation, based on changes in absorption. We prepared two types of samples referred to as sample A and sample B. In sample A (B), the SP-PS photochromic (SB35-PS absorptive) layer was used for the HLG layer and the SB35-PS absorptive (SP-PS photochromic) layer for the PWG layer. Therefore, in sample A, the HLG mode can be modulated by UV irradiation, while in sample B, it is the PWG mode that can be modulated.

All of the above-mentioned layers are fabricated by the spin coating method on cleaned SF11 substrates $15 \times 18 \times 1\ \text{mm}^3$ in size. For sample A, a toluene solution of a mixture of SP and PS (PS/solution = 6 wt. %, SP/PS = 10 wt. %) was first spun at a speed of 2500 rpm. Then, a water solution of PVA (7 wt. %) was spun at 2000 rpm. Finally, a toluene solution of a mixture of SB35 and PS (PS/solution = 6 wt. %, SB35/PS = 0.0125 wt. %) was spun at 2000 rpm. For sample B, on a cleaned SF11 substrate, a toluene solution of a mixture of SB35 and PS (PS/solution = 6 wt. %, SB35/PS = 0.5 wt. %) was first spun at a speed of 2000 rpm. Then, a water solution of PVA (7 wt. %) was spun at 2000 rpm. Finally, a toluene solution of a mixture of SP and PS (PS/solution = 6 wt. %, SP/PS = 3 wt. %) was spun at 2800 rpm. To remove the remaining solvent, after each spin coating of the layers, the samples were baked in air on a hot plate at 50 °C for 30 min.

The optical setup used for angle-scan ATR measurements is shown in Fig. 1(d). A probe light, an *s*-polarized light beam from a He–Ne laser with a wavelength of 632.8 nm, was incident on the sample through the SF11 prism. The sample was mounted on a computer-controlled rotation stage. The intensity of the reflected light coming out of the prism was measured with a photomultiplier connected to a lock-in amplifier as a function of the angle of incidence. The angle-scan reflectance spectra were obtained by dividing the intensity data recorded for the sample by those recorded for a bare part of the SF11 prism. To induce the photochromic reaction in the SP-PS layer, the sample was irradiated by unpolarized UV light from the air side as schematically shown in Fig. 1(d). We used a UV-LED (NICHIA, NVSU233A) that emits light with a relatively narrow emission band peaking at a wavelength of 365 nm with a full width at half maximum of ∼10 nm. We irradiated the whole surface of the sample by the LED placed ∼15 cm away from the sample. Under this irradiation condition, we could achieve uniform irradiation, and the variation of the power density over the sample surface was estimated to be less than 1%. For controlling the ATR spectra, the power densities on the samples were set to $0.28\ \text{mW/cm}^2$ for sample A and $0.11\ \text{mW/cm}^2$ for sample B, respectively. To minimize the photochromic reaction back to the closed-ring SP form induced by the probe beam (He–Ne laser beam), the power density of the probe beam was attenuated by a neutral density filter down to $14\ \text{nW/cm}^2$. The measurement was performed in a dark room, and the temperature during the measurement was ∼20 °C.

We performed systematic ATR measurements by repeating a cycle of the ATR measurement and UV irradiation. First, an initial ATR measurement was performed without UV irradiation. Then, the sample was irradiated by UV light with a constant power density during a certain period of time. After completing the angle-scan ATR measurement in dark within 3 min, the sample was again irradiated by UV light during another period of time. Afterward, the cycle of the ATR measurement and UV irradiation was repeated until the total irradiation time becomes sufficiently long. In this work, the amount of UV irradiation is expressed in terms of the dose given by a product of the irradiation power density (constant) and the accumulated irradiation time.

III. RESULTS AND DISCUSSION

A. Results of ATR measurements

Figure 2(a) shows the results of the ATR measurement for sample A, in which the photochromic SP-PS layer is implemented for the HLG layer as schematically shown in the upper part of the figure. We see that the ATR line shape changes drastically depending on the dose of UV irradiation. Without UV irradiation, the reflectance spectrum exhibits a sharp resonance dip around 60.0° with a width of ∼0.2° superposed on a broad and weak background extending over the whole angle range between 58.0° and 62.6°. Under UV irradiation, a broad resonance dip with a width larger than ∼2° emerges and the broad dip becomes deeper and broader as the UV dose increases. In parallel with the growth of the broad dip, the sharp resonance located around ∼60.0° changes its line shape dramatically. In general, for a multilayer sample, energy conservation requires $R + A + T = 1$, where R, A, and T are the

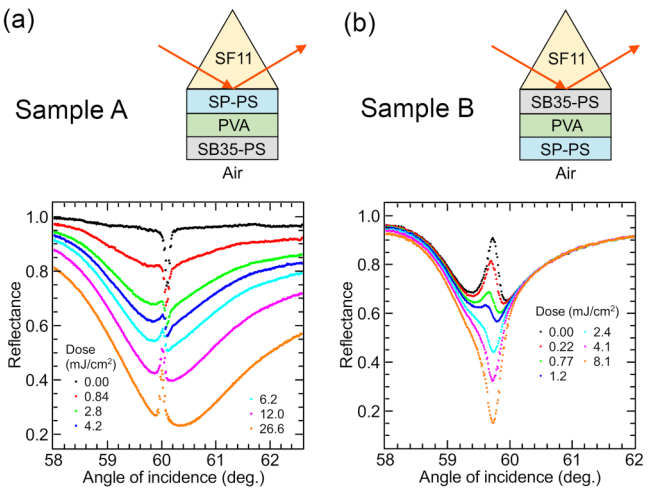

FIG. 2. ATR spectra of sample A (a) and sample B (b), measured before and after UV irradiation of various doses.

reflectance, absorptance, and transmittance, respectively. Since ATR spectra are measured under the total reflection condition, $T = 0$ holds and, consequently, reflectance spectra can be converted into absorptance spectra by $A = 1 - R$. As discussed in detail in our previous papers,[40,44] the absorptance of a multilayer sample is determined by a total absorption, i.e., a summation of absorption in all layers. It is thus convenient to discuss the observed line shape in terms of the absorptance spectra rather than the reflectance spectra.

When the reflectance spectra observed for the UV doses of 0.00–0.84 mJ/cm^2 shown in Fig. 2(a) are converted into the absorptance spectra, their spectral shapes can be classified into EIA-like spectra exhibiting a sharp absorption peak superposed on a broad absorption peak. For the doses from 2.8 to 6.2 mJ/cm^2, we find asymmetric Fano-like line shapes with a minimum at the low-angle side and a maximum at the high-angle side. Furthermore, the absorptance spectra of the doses of 12.0 and 26.6 mJ/cm^2 can be classified into EIT-like spectra exhibiting a sharp dip (suppression of absorption) in a broad absorption peak. The results presented in Fig. 2(a) indicate that a wide-range control of the line shape from the EIA-like to EIT-like line shape passing through the Fano-like line shape could be realized by UV irradiation.

Figure 2(b) shows the results of the ATR measurement for sample B in which the photochromic SP-PS layer is implemented for the PWG layer as schematically shown in the upper part of the figure. We see again that the ATR line shape changes drastically depending on the UV dose. When the spectra are converted to the absorptance spectra, the observed line shape can also be classified into three types. For the doses of 0.00 and 0.22 mJ/cm^2, the EIT-like line shape first appears. For the doses of 0.77 and 1.2 mJ/cm^2, the line shape turns to the Fano-like line shape. Finally, the spectra show the EIA-like line shape for the doses from 2.4 to 8.1 mJ/cm^2. From Fig. 2(b), it is clear that a wide-range control of the line shape from the EIT-like to EIA-like line shape was realized also in sample B. Compared to the spectra of sample A, the central resonance features in the spectra of sample B are slightly broader, while the background absorption is sharper.

As mentioned in Sec. II, MC molecules in the photochromic layers generated by UV irradiation can be thermally backconverted to SP molecules in dark. We checked the influence of the backconversion on the absorption in a single SP-PS layer deposited on a glass substrate, once irradiated by UV light and kept in dark. We found that the absorptance of the single layer decreases over time almost linearly ~8.5% in 3 min. The time needed to record an angle-scan ATR spectrum is approximately 3 min. Therefore, the influence of backconversion on the observed ATR spectra cannot be completely neglected. However, the time needed to scan the angle region around the central sharp resonance is less than ~1/10 of the total scan time. This means that the resonance features seen at the central part of the spectra in Figs. 2(a) and 2(b) are free from the deformation caused by the backconversion.

In our previous work,[44] we reported on the light control of the Fano-like resonance in a multilayer structure similar to the present sample A; no study was made on the structure analogous to sample B. As a light-controllable HLG layer, we used a PS layer doped with photochromic DR1 molecules. We note here that the presently observed change in the ATR line shape for sample A is much larger than that observed in our previous work. In fact, only the Fano-like line shape was observed in our previous work, while in the present work, the continuous change of the line shape from the EIA-like to the EIT-like line shape through the Fano-like line shape was realized. As discussed in detail later, the wide controllability of the line shape in the present study stems from a large change in the extinction coefficient of the HLG layer ($\Delta\kappa_{HLG}$), roughly twice as large as that in our previous work.[44] We also note that as in our previous studies on all-dielectric multilayer samples,[40,44] all the line shapes observed in the present work could be very well reproduced by the generalized Fano function proposed by Gallinet and Martin.[70,71]

B. EM analyses of line shapes

1. Estimation of structural parameters

To analyze the presently observed changes in the ATR spectra based on the EM theory, we need the values of the structural parameters (thicknesses and optical constants of the layers used). We estimated the values by fitting the observed ATR spectra to theoretical ones; to calculate the theoretical spectra, we used a freely available WinSpall software package,[72] which allows us to calculate the angle-dependent reflectance spectra of multilayer structures based on Fresnel reflection and transmission coefficients by varying the structural parameters. Values of the structural parameters that reproduce well the experimental spectra were searched. In the present fitting procedures, the refractive index of the SF11 prism at $\lambda = 632.8$ nm was set to $n_p = 1.7786$.[73] In Figs. 3(a) and 3(b), the

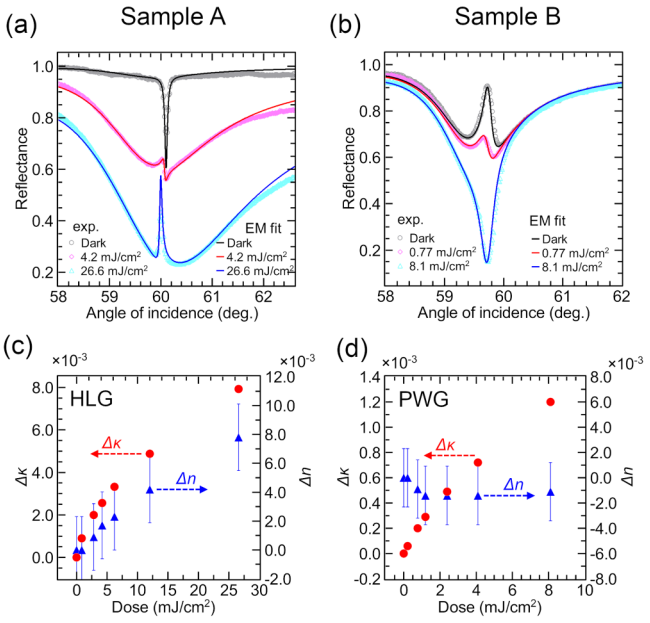

FIG. 3. Experimental ATR spectra (dots) and EM fit curves (solid) for sample A (a) and sample B (b). Variation of refractive index Δn and extinction coefficient $\Delta\kappa$ of the SP-PS photochromic layer of sample A (c) and sample B (d) estimated from EM fitting.

TABLE I. Structural parameters of sample A before UV irradiation.

Layer	Thickness d (nm)	Refractive index n	Extinction coefficient κ
HLG (SP-PS)	458	1.5960	2.3×10^{-4}
Spacer (PVA)	964	1.5240	1.0×10^{-5}
PWG (SB35-PS)	490	1.5866	6.5×10^{-5}

experimental spectra for sample A and sample B before (dark) and after UV irradiation are compared with the EM fit curves. We see that for both sample A and sample B, the EM fit curves reproduce well the experimental ATR spectra. The structural parameters obtained for the dark spectra of sample A and sample B are given in Tables I and II, respectively. To reproduce the experimental spectra of sample A after UV irradiation, the optical constants of the HLG layer (photochromic layer) were changed from the dark ones to $n_{HLG} = 1.5977$ and $\kappa_{HLG} = 2.8 \times 10^{-3}$ for 4.2 mJ/cm^2 and $n_{HLG} = 1.6038$ and $\kappa_{HLG} = 8.15 \times 10^{-3}$ for 26.6 mJ/cm^2. For sample B after UV irradiation, the optical constants of the PWG layer (photochromic layer) were changed to $n_{PWG} = 1.5809$ and $\kappa_{PWG} = 2.35 \times 10^{-4}$ for 0.77 mJ/cm^2 and $n_{PWG} = 1.5807$ and $\kappa_{PWG} = 1.235 \times 10^{-3}$ for 8.1 mJ/cm^2. The EM fitting was successful for all the spectra observed under different UV doses and allowed us to trace the variation in the optical constants of the photochromic SP-PS layer as a function of the UV dose.

Differences of the refractive index and extinction coefficient from their dark values, Δn and $\Delta\kappa$, for the SP-PS photochromic layer are plotted as a function of the UV dose in Figs. 3(c) and 3(d) for sample A and sample B, respectively. The experimental error in Δn was estimated from an amount of fluctuation in the angular position of a sharp ATR dip; for this estimation, the ATR measurement was repeated over 20 times for an ATR sample exhibiting a very sharp dip corresponding to the excitation of a PWG mode in a pure PS waveguide layer. Although the fluctuation in the intensity of reflected light during the ATR measurement (±∼2%) can be a source of error in determining κ and $\Delta\kappa$, the error in $\Delta\kappa$ was found to be of the same order of magnitude as the size of the data points in Figs. 3(c) and 3(d).

Figure 3(c) shows that both the extinction coefficient κ and the refractive index n in the SP-PS layer of sample A increase monotonically, as the UV dose increases; for the dose of 26.6 mJ/cm^2, Δn takes a value of 7.8×10^{-3}, while $\Delta\kappa$ takes a value of 7.92×10^{-3}. The results shown in Fig. 3(c) are in good qualitative agreement with those previously reported for SP molecules embedded in polymer films.[58,59,68] However, quantitative comparisons of Δn and $\Delta\kappa$ values with literature values are difficult because of differences in the SP concentration and the host polymer used, as well as the different UV irradiation condition. Figure 3(d) shows that $\Delta\kappa$ in sample B is 1.2×10^{-3} for the dose of 8.1 mJ/cm^2. This value is roughly five times smaller than the corresponding value in sample A for the same UV dose. This smaller value is mainly caused by a smaller concentration of SP molecules in sample B (SP/PS 3 wt. %) relative to sample A (SP/PS 10 wt. %). Δn for sample B is very small, falling in the range of the experimental error of $\pm 2.3 \times 10^{-3}$. Figures 3(c) and 3(d) demonstrate that the extinction coefficient of the SP-PS photochromic layer in sample A and sample B at the wavelength of 632.8 nm can be controlled systematically by changing the dose of UV irradiation.

TABLE II. Structural parameters of sample B before UV irradiation.

Layer	Thickness d (nm)	Refractive index n	Extinction coefficient κ
HLG (SB35-PS)	496	1.5810	1.7×10^{-3}
Spacer (PVA)	980	1.5294	1.0×10^{-5}
PWG (SP-PS)	438	1.5818	3.5×10^{-5}

2. Mechanism of line shape changes

To clarify the mechanism of changes in the ATR line shape, we have to know how the absorption in each layer changes depending on the UV dose. According to the EM theory,[74] the energy of light absorbed per unit time and unit volume in the vicinity of a point $\mathbf{r} = (x, y, z)$ in an absorptive medium is proportional to $\varepsilon_2|\mathbf{E}(\mathbf{r})|^2$, where $\varepsilon_2 = 2n\kappa$ represents the imaginary part of the dielectric constant of the medium and $|\mathbf{E}(\mathbf{r})|$ is the magnitude of the electric field generated at the position $\mathbf{r}$. We calculated the electric field distributions in our multilayer samples generated by the probe light with $\lambda = 632.8$ nm in a form of the field enhancement factor (FEF), $|E(z, \theta_{pr})|^2/|E_0|^2$, where $|E(z, \theta_{pr})|$ denotes the magnitude of electric field generated at the position z at the angle of incidence θ_{pr}, while $|E_0|$ denotes that of the incident light. A plane wave was assumed to be incident on the multilayer sample through the prism, and the calculation was performed using a 2×2 transfer-matrix method[75] together with the structural parameters obtained by the EM fitting described in Subsection III B 1. The results of the calculations are summarized in the supplementary material, and FEF are plotted as functions of position z in the samples and angle of incidence θ_{pr} in Figs. S1 and S2 in the supplementary material for sample A and sample B, respectively.

The color maps of FEF (see Figs. S1 and S2 in the supplementary material) demonstrate that in the HLG layer, moderately enhanced local electric fields (with a maximum FEF of ∼20) are generated over a wide angle range, where the ATR spectra of sample A and sample B (Fig. 3) exhibit a broad dip; the generation of the broad distributions is due to the excitation of the HLG mode. They also show that in the PWG layer, highly enhanced local electric fields (with a maximum FEF of ∼450) are generated in a narrow angle range, where the ATR spectra exhibit sharp resonant features; this is due to the excitation of the PWG mode. A remarkable feature seen in the distributions is a strong suppression of the local electric fields inside the HLG layer in the narrow angle range corresponding to the PWG mode excitation. The suppression of the fields is a direct consequence of the coupling between the HLG and PWG modes.[44] In addition, the color maps of FEF also indicate that as the UV dose increases, the overall FEF decreases because of the increase in the extinction coefficient of the photochromic layer.

Now, we proceed to the calculation of absorption spectra in the respective layers. As in our previous work,[44] we consider the energy flow of light incident on a unit area of the prism–sample interface.

To evaluate the energy absorbed in a layer, we take a volume terminated by unit areas on the interfaces at both sides of the layer. The ratio of the energy absorbed in that volume of the layer to the energy of incident light per unit area is given by $C(\cos\theta_{pr})^{-1}\int\varepsilon_2|E(z,\theta_{pr})|^2/|E_0|^2\,dz$, where C is a constant, θ_{pr} is the angle of incidence of the probe light (inside the prism), and the integration is taken over the thickness of the layer. The factor $(\cos\theta_{pr})^{-1}$ accounts for the variation of the incident energy per unit area. In the calculation, we used the structural parameters determined in Subsection III B 1 and the numerical results of FEF. For simplicity, C was taken to be unity. Figure 4(a) shows the calculated absorption spectra for sample A corresponding to the UV doses of 0.00 (dark), 4.2, and 26.6 mJ/cm^2, while Fig. 4(b) shows those for sample B corresponding to the UV doses of 0.00 (dark), 1.2, and 4.1 mJ/cm^2. In the figures, the absorption spectra $A_{HLG}(\theta_{pr})$, $A_{Spacer}(\theta_{pr})$, and $A_{PWG}(\theta_{pr})$ in the HLG, Spacer, and PWG layers, respectively, are shown together with the total absorption spectra $A_{Total}(\theta_{pr})$. Note that when the proportionality constant C is well adjusted, $A_{Total}(\theta_{pr})$ reproduces the absorptance spectra well converted from the ATR spectra.

Figures 4(a) and 4(b) reveal that the contribution of $A_{Spacer}(\theta_{pr})$ to $A_{Total}(\theta_{pr})$ is quite small and $A_{Total}(\theta_{pr})$ is determined mainly by $A_{HLG}(\theta_{pr})$ and $A_{PWG}(\theta_{pr})$. The small values of $A_{Spacer}(\theta_{pr})$ stem from the local electric fields rapidly decaying away from the PWG/Spacer interface (see Figs. S1 and S2 in the supplementary material) and very small extinction coefficients (Tables I and II) in the PVA Spacer layer. For sample A, Fig. 4(a) shows that under dark, $A_{PWG}(\theta_{pr})$ exhibits a strong Lorentzian-like sharp peak around 60° corresponding to the excitation of PWG mode, while $A_{HLG}(\theta_{pr})$ exhibits a weak dip at the same position; the contribution of $A_{PWG}(\theta_{pr})$ dominates and consequently, $A_{Total}(\theta_{pr})$ exhibits a sharp Lorentzian-like peak superposed on a weak broad background (EIA-like spectrum). Under UV irradiation, $A_{PWG}(\theta_{pr})$ still exhibits a sharp Lorentzian-like peak, but its intensity decreases as the UV dose increases [panels of 4.2 and 26.6 mJ/cm^2 in Fig. 4(a)]. On the other hand, the overall intensity of $A_{HLG}(\theta_{pr})$ increases remarkably while keeping the EIT-like line shape. It should be noted that the EIT-like line shape in $A_{HLG}(\theta_{pr})$ is caused by the suppression of the local electric fields inside the HLG layer around the excitation angle of the PWG mode. For the dose of 4.2 mJ/cm^2, $A_{PWG}(\theta_{pr})$ and $A_{HLG}(\theta_{pr})$ contribute to $A_{Total}(\theta_{pr})$ with almost equal weights, resulting in the Fano-like line shape in $A_{Total}(\theta_{pr})$. For the dose of 26.6 mJ/cm^2, the contribution of $A_{HLG}(\theta_{pr})$ is dominant, leading to the EIT-like line shape in $A_{Total}(\theta_{pr})$. Figure 4(a) clearly demonstrates that the changes in the line shape of $A_{Total}(\theta_{pr})$ is caused by the change in the relative contributions of $A_{PWG}(\theta_{pr})$ and $A_{HLG}(\theta_{pr})$.

Figure 4(b) also demonstrates clearly the changes in the relative contributions of $A_{PWG}(\theta_{pr})$ and $A_{HLG}(\theta_{pr})$ for sample B. Under dark, the contribution of $A_{HLG}(\theta_{pr})$ with a EIT-like line shape dominates and, consequently, $A_{Total}(\theta_{pr})$ exhibits the EIT-like line shape. Under UV irradiation, the intensity of $A_{HLG}(\theta_{pr})$ remains almost the same, while that of $A_{PWG}(\theta_{pr})$ with a sharp Lorentzian-like peak increases remarkably as the UV dose increases. Consequently, the almost equal contributions of $A_{PWG}(\theta_{pr})$ and $A_{HLG}(\theta_{pr})$ result in the Fano-like line shape in $A_{Total}(\theta_{pr})$ for the UV dose of 1.2 mJ/cm^2 and the dominant contribution of $A_{PWG}(\theta_{pr})$ leads to the EIA-like line shape for the UV dose of 4.1 mJ/cm^2. From Figs. 4(a) and 4(b), it is now clear that the changes in the line shape from the EIA-like to EIT-like (or vice versa) through the Fano-like line shape is brought by the remarkable increase in the absorption of the photochromic layer, i.e., the HLG layer in sample A and the PWG layer in sample B. As the UV dose increases, the extinction coefficients of the photochromic layers strongly increase [Figs. 3(c) and 3(d)] and simultaneously the amplitudes of local electric fields inside the layers moderately decrease (see Figs. S1 and S2 in the supplementary material). Even with the decrease in the local electric fields, the absorption in the layers increases remarkably, because the increase in ε_2 overcomes the decrease in the local electric fields. In fact, for both sample A and sample B, FEF decreases down to a half, but ε_2 increases by a factor larger than 10.

Although the observed changes in the ATR line shape can be well explained in a manner described above, we suggest here an alternative physical picture for understanding the observed phenomena. As explained in detail in textbooks for the SPP excitation,[76,77] the generation of a dip in ATR spectra can be explained in terms of the excitation of an electromagnetic mode (SPP) by a wave incident from a prism (incoupling process) and the reradiation of a wave into the prism from the excited electromagnetic mode (SPP) (outcoupling process). The dip in the reflection spectrum is a consequence of a destructive interference between the reradiated wave that exhibits a resonant behavior due to the

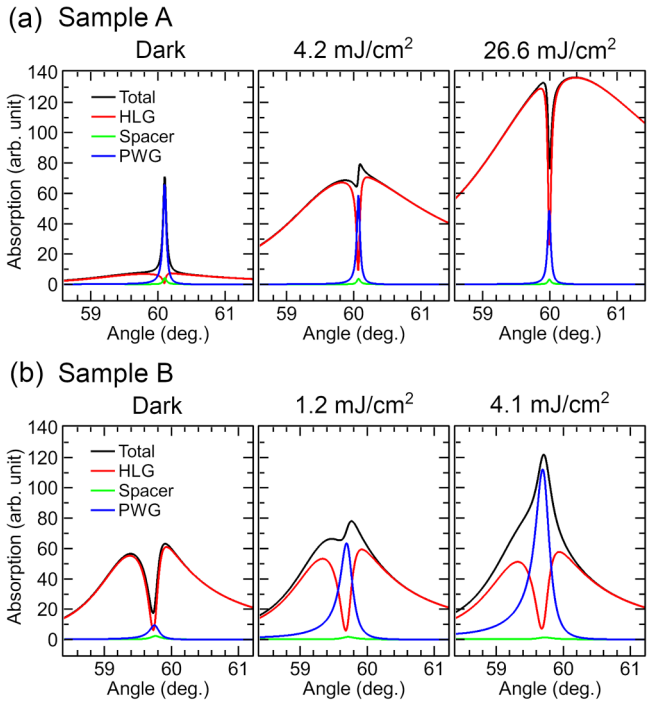

FIG. 4. Absorption spectra of respective layers and total absorption spectra for sample A (a) and sample B (b) calculated using structural parameters estimated from the EM fitting.

excitation of the mode and a nonresonant reflected wave that is not influenced by the excitation of the mode. In our recent theoretical work,[78] taking these processes into account, we have developed a coupled-mode theory for the SPP excitation and discussed the ATR response in both Kretschmann and Otto configurations. We demonstrated that the numerical results of the coupled-mode theory agree fairly well with those of rigorous EM calculations.

The all-dielectric multilayer structures studied in this work support two different modes, HLG and PWG modes, that interact with each other and form coupled modes. The incoupling and outcoupling processes take place for the coupled modes. The presently observed changes in the ATR line shape induced by the absorption changes in the photochromic layers may be explained mainly by the changes in the relative contributions of intrinsic damping of the HLG and PWG modes to the coupled mode, even though the incoupling and outcoupling processes, the radiation damping, and the intercoupling of the modes may also be affected. Very recently,[79] we have extended the coupled-mode theory to the case of interacting SPP and PWG modes in metal–dielectric multilayer structures that generate Fano-like line shapes. The extension of the theory to the present structure involving the HLG and PWG modes is straightforward and is currently under way. The formulation and numerical results applied to the present sample structures will be published elsewhere.

C. Enhanced absorption change in Fano-resonant multilayer structure

The present results of ATR measurements shown in Fig. 2 indicate that UV irradiation of the sample can induce a very large change in the absorption when the photochromic layer is incorporated into the Fano-resonant multilayer structure. Since the absorption change in sample B around the Fano-like resonance is especially large, we focus on and discuss the drastic absorption change in sample B. To see more clearly the change in the absorption in sample B, the change in the absorptance ΔA at the resonance angle of 59.73° obtained from the relation $A = 1 - R$ is plotted in Fig. 5 as a function of the UV dose. We can see a large change in the absorptance varying from 0 to ∼0.8 as the UV dose increases from 0 to 8.1 mJ/cm^2. This change in ΔA is caused by the increase in the extinction coefficient κ of the SP-PS photochromic layer incorporated as the PWG layer in sample B; $\Delta\kappa$ for the dose of 8.1 mJ/cm^2 is 1.2×10^{-3} [Fig. 3(d)]. When a single SP-PS photochromic layer is deposited on a SF11 substrate, referred to as the SL sample, ΔA as large as 0.8 cannot be achieved by the same amount of $\Delta\kappa$. We theoretically calculated ΔA for the SL sample assuming a plane wave of $\lambda = 632.8$ nm incident normal to the sample surface from the SF11 substrate; the WinSpall software package was again used together with the thickness and optical constants of the photochromic layer identical to those in sample B. The calculated dependence of ΔA on the UV dose is plotted in Fig. 5. We see that ΔA of the SL sample is as small as $\sim 1.0 \times 10^{-2}$ even for the maximum dose of 8.1 mJ/cm^2. Comparing ΔA of sample B with that of the SL sample, we find that ΔA of sample B is highly enhanced (by a factor of ∼100) relative to that of the SL sample.

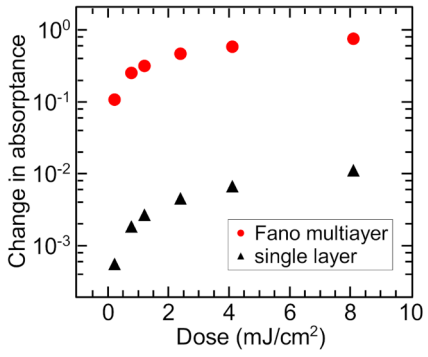

FIG. 5. Comparison of change in absorptance in the Fano multilayer structure and a single photochromic layer. The data of Fano-resonant multilayer structure were extracted from the experimentally obtained ATR spectra of sample B (at 59.73°). The data of the single layer were calculated using the same optical constants as those estimated from the EM fitting of sample B.

It is very much plausible that the enhanced photochromic response detected as ΔA in the present multilayer structure is caused by the enhanced local electric fields inside the photochromic layer. There are two possibilities of the field enhancement, i.e., in the excitation and probe processes. We have calculated the electric field distributions settled in sample B and the SL sample by the UV excitation light ($\lambda = 365$ nm) incident normal to the sample surface from the air side, in a manner very similar to that described in Subsection III B 2. We found that in both sample B and the SL sample, FEF inside the photochromic layers take values less than ∼0.7 and average values of FEF are almost the same for sample B and the SL sample (difference is only ∼2%). Therefore, UV irradiation from the air side of the samples induces almost the same changes in the optical constants of the photochromic layers and the field enhancement in the excitation process cannot be the origin of the enhanced ΔA.

In Subsection III B 2, we have already discussed the enhancement in the local electric fields inside the photochromic layer generated by the probe light (the maps of FEF for sample B are given in Fig. S2 in the supplementary material). To clarify the behavior of FEF in sample B at the angle of 59.73°, FEF is plotted as a function of the position z [see Fig. S3(a) in the supplementary material]. The electric field profiles demonstrate that highly enhanced local electric fields are generated in the photochromic layer due to the excitation of the PWG mode. Although the average of FEF over the layer decreases as the UV dose increases, it is still as high as ∼50. Combined with the strong increase in ε_2, the absorption in the photochromic layer strongly increases [$A_{\mathrm{PWG}}(\theta_{\mathrm{pr}})$ in Fig. 4(b)], finally yielding large changes in ΔA plotted in Fig. 5. We also calculated the electric field profiles generated in the SL sample by the probe light [see Fig. S3(b) in the supplementary material]. In contrast to sample B, the average FEF in the photochromic layer in the SL sample is ∼1.2 and does not depend appreciably on the UV dose. Since the UV excitation from the air side induces almost the same increase in ε_2 of the photochromic layer in sample B and the SL sample, we can finally conclude that the highly enhanced ΔA for sample B relative to that of the SL sample seen in Fig. 5 is caused by the large enhancement of local electric fields inside the photochromic layer in sample B.

IV. CONCLUSIONS

Using the SP-PS photochromic layer as one of the waveguide layers in all-dielectric multilayer structures, we have succeeded in controlling the ATR line shape in a wide range by UV irradiation. In one of the present samples, the SP-PS photochromic layer was used for the HLG layer, and in another sample, the photochromic layer was implemented as the PWG layer. The line shape in the absorptance spectra converted from the ATR spectra drastically changed from the EIA-like to EIT-like line shape (or vice versa) passing through the Fano-like line shape, as the dose of UV irradiation increased. To the best of our knowledge, the light control of the Fano-like resonances in such a wide range has not been reported so far. The photoinduced changes in the absorptance ΔA observed are much larger than those in the single layer of the same SP-PS photochromic layer deposited on a glass substrate.

Using calculated distributions of local electric fields and estimated imaginary parts of the dielectric constants in the respective layers, we calculated the absorption spectra in the layers. It was found that the line shape of the total absorption spectrum is determined by the contributions of the EIT-like spectrum of the HLG layer and the Lorentzian-like spectrum of the PWG layer. The wide-range change in the line shape observed can be well explained by the large increase in the absorption in the photochromic HLG or PWG layer. Furthermore, the results of our EM analyses suggest that the enhanced photochromic responses observed for the Fano-resonant multilayer structure is due to the enhanced local electric fields inside the photochromic waveguide layer upon excitation of the PWG mode. The active line shape control by light as well as the large modulation of optical signals (reflectance and absorptance) demonstrated in this work may open up new avenues to extend the potential applications of the photochromic layer, such as all-optic switches, optical filters, optical memories, and biosensors. Optical responses similar to those presented in this paper are expected to be realized also in the wavelength-scan ATR spectra and are currently under investigation by our group.

SUPPLEMENTARY MATERIAL

See the supplementary material for FEF in sample A and sample B and the comparison of FEF in sample B and the SL sample.

ACKNOWLEDGMENTS

This work was supported by JSPS KAKENHI (Grant Nos. 19K05307 and 16H03828).

REFERENCES

[1]U. Fano, Il Nuovo Cim. **12**, 154 (1935).
[2]U. Fano, Phys. Rev. **124**, 1866 (1961).
[3]K.-J. Boller, A. Imamoğlu, and S. E. Harris, Phys. Rev. Lett. **66**, 2593 (1991).
[4]S. E. Harris, Phys. Today **50**(7), 36 (1997).
[5]M. Fleischhauer, A. Imamoglu, and J. P. Marangos, Rev. Mod. Phys. **77**, 633 (2005).
[6]A. M. Akulshin, S. Barreiro, and A. Lezama, Phys. Rev. A **57**, 2996 (1998).
[7]A. Lezama, S. Barreiro, and A. M. Akulshin, Phys. Rev. A **59**, 4732 (1999).
[8]A. V. Taichenachev, A. M. Tumaikin, and V. I. Yudin, Phys. Rev. A **61**, 011802 (1999).
[9]A. E. Miroshnichenko, S. Flach, and Y. S. Kivshar, Rev. Mod. Phys. **82**, 2257 (2010).
[10]B. Luk'yanchuk, N. I. Zheludev, S. A. Maier, N. J. Halas, P. Nordlander, H. Giessen, and C. T. Chong, Nat. Mater. **9**, 707 (2010).
[11]M. F. Limonov, M. V. Rybin, A. N. Poddubny, and Y. S. Kivshar, Nat. Photonics **11**, 543 (2017).
[12]Q. Xu, S. Sandhu, M. L. Povinelli, J. Shakya, S. Fan, and M. Lipson, Phys. Rev. Lett. **96**, 123901 (2006).
[13]S. Zhang, D. A. Genov, Y. Wang, M. Liu, and X. Zhang, Phys. Rev. Lett. **101**, 047401 (2008).
[14]N. Liu, L. Langguth, T. Weiss, J. Kästel, M. Fleischhauer, T. Pfau, and H. Giessen, Nat. Mater. **8**, 758 (2009).
[15]P. Tassin, L. Zhang, R. Zhao, A. Jain, T. Koschny, and C. M. Soukoulis, Phys. Rev. Lett. **109**, 187401 (2012).
[16]R. Taubert, M. Hentschel, J. Kästel, and H. Giessen, Nano Lett. **12**, 1367 (2012).
[17]R. Taubert, M. Hentschel, and H. Giessen, J. Opt. Soc. Am. B **30**, 3123 (2013).
[18]F. Hao, Y. Sonnefraud, P. Van Dorpe, S. A. Maier, N. J. Halas, and P. Nordlander, Nano Lett. **8**, 3983 (2008).
[19]R. Singh, W. Cao, I. Al-Naib, L. Cong, W. Withayachumnankul, and W. Zhang, Appl. Phys. Lett. **105**, 171101 (2014).
[20]W. S. Chang, J. B. Lassiter, P. Swanglap, H. Sobhani, S. Khatua, P. Nordlander, N. J. Halas, and S. Link, Nano Lett. **12**, 4977 (2012).
[21]L. Stern, M. Grajower, and U. Levy, Nat. Commun. **5**, 4865 (2014).
[22]Y. Yang, W. Wang, A. Boulesbaa, I. I. Kravchenko, D. P. Briggs, A. Puretzky, D. Geohegan, and J. Valentine, Nano Lett. **15**, 7388 (2015).
[23]J. Ye, F. Wen, H. Sobhani, J. B. Lassiter, P. Van Dorpe, P. Nordlander, and N. J. Halas, Nano Lett. **12**, 1660 (2012).
[24]A. Nazir, S. Panaro, R. Proietti Zaccaria, C. Liberale, F. De Angelis, and A. Toma, Nano Lett. **14**, 3166 (2014).
[25]B. Lee, J. Park, G. H. Han, H. S. Ee, C. H. Naylor, W. Liu, A. T. C. Johnson, and R. Agarwal, Nano Lett. **15**, 3646 (2015).
[26]X. Zhang, S. Choi, D. Wang, C. H. Naylor, A. T. C. Johnson, and E. Cubukcu, Nano Lett. **17**, 6715 (2017).
[27]W. Wang, A. Klots, Y. Yang, W. Li, I. I. Kravchenko, D. P. Briggs, K. I. Bolotin, and J. Valentine, Appl. Phys. Lett. **106**, 181104 (2015).
[28]Y. Jung, I. Hwang, J. Yu, J. Lee, J. H. Choi, J. H. Jeong, J. Y. Jung, and J. Lee, Sci. Rep. **9**, 7834 (2019).
[29]A. D. Boardman, in *Electromagnetic Surface Modes* (John Wiley & Sons, Chichester, 1982).
[30]A. Yariv and P. Yeh, *Optical Waves in Crystals Propagation and Control of Laser Radiation* (Wiley, New York, 2002).
[31]H. Grotewohl and M. Deutsch, J. Opt. **17**, 085003 (2015).
[32]Y. Neo, T. Matsumoto, T. Watanabe, M. Tomita, and H. Mimura, Opt. Express **24**, 26201 (2016).
[33]K. Matsunaga, T. Watanabe, Y. Neo, T. Matsumoto, and M. Tomita, Opt. Lett. **41**, 5274 (2016).
[34]K. Matsunaga, Y. Hirai, Y. Neo, T. Matsumoto, and M. Tomita, Sci. Rep. **7**, 17824 (2017).
[35]S. Hayashi, D. V. Nesterenko, and Z. Sekkat, Appl. Phys. Express **8**, 022201 (2015).
[36]S. Hayashi, D. V. Nesterenko, and Z. Sekkat, J. Phys. D. Appl. Phys. **48**, 325303 (2015).
[37]D. V. Nesterenko, S. Hayashi, and Z. Sekkat, J. Opt. **18**, 065004 (2016).
[38]S. Hayashi, D. V. Nesterenko, A. Rahmouni, and Z. Sekkat, Appl. Phys. Lett. **108**, 051101 (2016).
[39]S. Hayashi, Y. Fujiwara, B. Kang, M. Fujii, D. V. Nesterenko, and Z. Sekkat, J. Appl. Phys. **122**, 163103 (2017).
[40]B. Kang, M. Fujii, D. V. Nesterenko, Z. Sekkat, and S. Hayashi, J. Opt. **20**, 125003 (2018).
[41]S. Hayashi, D. V. Nesterenko, A. Rahmouni, H. Ishitobi, Y. Inouye, S. Kawata, and Z. Sekkat, Sci. Rep. **6**, 33144 (2016).

[42]S. Hayashi, D. V. Nesterenko, A. Rahmouni, and Z. Sekkat, Phys. Rev. B **95**, 165402 (2017).
[43]S. Hayashi, D. V. Nesterenko, and Z. Sekkat, in *Fano Resonances in Optics and Microwaves*, edited by E. Kamenetskii, A. Sadreev, and A. Miroshnichenko (Springer, New York, 2018), pp. 241–260.
[44]K. Motokura, B. Kang, M. Fujii, D. V. Nesterenko, Z. Sekkat, and S. Hayashi, J. Appl. Phys. **125**, 223101 (2019).
[45]N. Jiang, X. Zhuo, and J. Wang, Chem. Rev. **118**, 3054 (2018).
[46]J. Sautter, I. Staude, M. Decker, E. Rusak, D. N. Neshev, I. Brener, and Y. S. Kivshar, ACS Nano **9**, 4308 (2015).
[47]Y. Cui, J. Zhou, V. A. Tamma, and W. Park, ACS Nano **6**, 2385 (2012).
[48]N. Dabidian, I. Kholmanov, A. B. Khanikaev, K. Tatar, S. Trendafilov, S. H. Mousavi, C. Magnuson, R. S. Ruoff, and G. Shvets, ACS Photonics **2**, 216 (2015).
[49]H. P. Xin, F. Liu, G. J. Ren, H. L. Zhao, and J. Q. Yao, Opt. Commun. **389**, 92 (2017).
[50]F. Chen, H. Zhang, L. Sun, J. Li, and C. Yu, Optik **185**, 585 (2019).
[51]A. Li and W. Bogaerts, Opt. Express **25**, 31688 (2017).
[52]F. Chen, H. Zhang, L. Sun, J. Li, and C. Yu, Opt. Laser Technol. **116**, 293 (2019).
[53]Y. Huang, J. Yan, C. Ma, and G. Yang, Nanoscale Horiz. **4**, 148 (2019).
[54]R. Yu, C. Ding, D. Zhang, and S. Zhang, J. Appl. Phys. **121**, 144303 (2017).
[55]R. Yahiaoui, M. Manjappa, Y. K. Srivastava, and R. Singh, Appl. Phys. Lett. **111**, 021101 (2017).
[56]X. Zhang, N. Biekert, S. Choi, C. H. Naylor, C. De-Eknamkul, W. Huang, X. Zhang, X. Zheng, D. Wang, A. T. C. Johnson, and E. Cubukcu, Nano Lett. **18**, 957 (2018).
[57]T. Schwartz, J. A. Hutchison, C. Genet, and T. W. Ebbesen, Phys. Rev. Lett. **106**, 196405 (2011).
[58]A. L. Baudrion, A. Perron, A. Veltri, A. Bouhelier, P. M. Adam, and R. Bachelot, Nano Lett. **13**, 282 (2013).
[59]W. M. Wilson, J. W. Stewart, and M. H. Mikkelsen, Nano Lett. **18**, 853 (2018).
[60]F. Yang and J. R. Sambles, J. Opt. Soc. Am. B **10**, 858 (1993).
[61]N. J. Smith and J. R. Sambles, J. Appl. Phys. **85**, 3984 (1999).
[62]N. W. Tyer and R. S. Becker, J. Am. Chem. Soc. **92**, 1289 (1970).
[63]S. A. Krysanov and M. V. Alfimov, Chem. Phys. Lett. **91**, 77 (1982).
[64]J. Buback, M. Kullmann, F. Langhojer, P. Nuernberger, R. Schmidt, F. Würthner, and T. Brixner, J. Am. Chem. Soc. **132**, 16510 (2010).
[65]R. Klajn, Chem. Soc. Rev. **43**, 148 (2014).
[66]H. Ishitobi, Z. Sekkat, and S. Kawata, Chem. Phys. Lett. **300**, 421 (1999).
[67]Z. Sekkat and W. Knoll, *Photoreactive Organic Thin Films* (Elsevier Science, Amsterdam, 2002).
[68]K. Sasaki and T. Nagamura, J. Appl. Phys. **83**, 2894 (1998).
[69]H. Eckhardt, A. Bose, and V. A. Krongauz, Polymer **28**, 1959 (1987).
[70]B. Gallinet and O. J. F. Martin, Phys. Rev. B **83**, 235427 (2011).
[71]B. Gallinet and O. J. F. Martin, ACS Nano **5**, 8999 (2011).
[72]RES-TEC, see www.res-tec.de for "Winspall Data Analysis Software" (accessed 23 September 2019).
[73]M. N. Polyanskiy, see https://refractiveindex.info for "Refractive Index Database" (accessed 23 September 2019).
[74]L. D. Landau and E. M. Lifshitz, *Electrodynamics of Continuous Media*, 1st ed. (Pergamon Press, Oxford, 1960), pp. 253–256.
[75]C. C. Katsidis and D. I. Siapkas, Appl. Opt. **41**, 3978 (2002).
[76]H. Raether, *Surface Plasmons on Smooth and Rough Surfaces and on Gratings* (Springer, Berlin, 1988), pp. 11–16.
[77]S. A. Maier, *Plasmonics Fundamentals and Applications* (Springer, New York, 2007), pp. 42–44.
[78]D. V. Nesterenko, S. Hayashi, and Z. Sekkat, Phys. Rev. B **97**, 235437 (2018).
[79]D. V. Nesterenko, J. Phys. Conf. Ser. **1368**, 052046 (2019).